Biochemical and Biophysical Research Communications 435 (2013) 651–656

Contents lists available at SciVerse ScienceDirect

Biochemical and Biophysical Research Communications

journal homepage: www.elsevier.com/locate/ybbrc

Changes of apoptosis in tumor tissues with time after irreversible electroporation

Hong-Bae Kim [a], Chang-Kyu Sung [a,*], Ku Youn Baik [b], Kee-Wook Moon [c], Hyung-Sik Kim [d], Jeong-Han Yi [d], Jong-Hyun Jung [e], Min-Hoan Moon [a], Ohc-Kyung Choi [a]

[a] Department of Radiology and Seoul National University Cancer Research Institute, Seoul National University College of Medicine, SNU-SMG Boramae Medical Center, 39 Boramae-Gil, Dongjak-Gu, Seoul 156-707, Republic of Korea
[b] Department of Electrical and Biological Physics, Kwangwoon University, 26 Kwangwoon-gil, Nowon-gu, Seoul 139-701, Republic of Korea
[c] Solco-Biomedical Institute, Solco-Biomedical Co. Ltd., 34-6 Geumam-ri, Seotan-myeon, Pyeongtaek, Gyeonggi-do 451-852, Republic of Korea
[d] Department of Biomedical Engineering, Research Institute of Biomedical Engineering, College of Biomedical & Health Science, Konkuk University, 322 Danwol-dong, Chung-ju-si, Chungcheongbuk-do 380-701, Republic of Korea
[e] Computational Nano-Materials Physics Lab., Department of Physics and Astronomy, Seoul National University, 1 Gwanak-ro, Gwanak-gu, Seoul 151-742, Republic of Korea

ARTICLE INFO

Article history:
Received 7 May 2013
Available online 17 May 2013

Keywords:
Irreversible electroporation
Apoptosis
Contrast-enhanced magnetic resonance image
Histological examination
Devascularization

ABSTRACT

Irreversible electroporation is a novel method of ablating living tissues through its non-thermal effects, unlike radiofrequency ablation which has a severe problem of heat sink. It is due to high-energy direct current which leads to permanent disruption of lipid bilayer integrity in terms of exchanges between intra- and extracellular components via nano-sized pores. That finally causes irreversible damage to cellular homeostasis. Irreversibly damaged cells may undergo apoptosis followed by necrosis with time after electroporation. This damage can make it possible to monitor the ablated area with time post-IRE through MR imaging and an ultrasound system. Most previous studies have investigated the immediate response of undesired tissue to IRE. In our study, we showed changes of tumor tissues with time post-IRE by histological analysis and MR imaging. Tissues under IRE ablation showed a peak apoptotic rate at 24 h after IRE ablation with viable tissues at the peripheral rim of treated tissues in histological analysis. This phenomenon was also observed with no enhancement on contrast-enhanced MR images due to devascularization of IRE ablated zones.

1. Introduction

Irreversible electroporation (IRE) has pervaded the clinical field since the report of application of IRE in ablating of pig's liver without harming surrounding tissues by the Rubinsky group [1]. IRE is a modality using microsecond electrical pulses across cells to induce permanent permeabilization of the cell membrane, after all, cell death if the applied power is high enough. IRE has been known to produce precisely delineated ablation zones with cell scale resolution between ablated and non-ablated areas, with preserved massive blood vessel congestion in the sinusoids of the treated region. IRE can be thus applied to ablate target tissues without affecting the surrounding normal tissue including blood vessels [2]. This localized ablation of IRE make it possible to immediately monitor the IRE treated region via histology, magnetic resonance image (MRI) [3,4] and an ultrasound system [5].

Previous studies have reported the immediate response of IRE treated tissues and have shown that IRE induced cell apoptosis and necrosis [3,4]. However, these changes should be followed by many other processes and it may last over one day. To monitor these changes with time *in vivo* is very important to assess IRE effects on tissues. Furthermore, previous studies have used normal animal organs or cancer cell lines, and few studies have used tumor tissues *in vivo*. Due to different properties of tissues, to apply IRE directly to tumor tissues is important for estimating the capacity of IRE for cancer therapy. In this pilot study, we assessed the changes within tumor tissues after IRE ablation with time by using histological analysis and MR imaging.

2. Materials and methods

2.1. Tumor cell line

The human prostate cancer line PC-3 was received from Korean Cell Line Bank and cultured in RPMI 1640 (ATCC) with L-glutamine (300 mg/L), 25 mM HEPES and 25 mM $NaHCO_3$ supplemented with 10% fetal bovine serum (Sigma–Aldrich). Cells were maintained in culture petri-dishes at 37 °C in a humidified atmosphere containing 5% CO_2. Before each implantation procedure, viability of the

* Corresponding author. Fax: +82 2 870 3539.
E-mail address: sckmd@naver.com (C.-K. Sung).

0006-291X/$ - see front matter © 2013 Elsevier Inc. All rights reserved.
http://dx.doi.org/10.1016/j.bbrc.2013.05.039

cells was tested through trypan blue staining (confirming >90% cell viability for each tumor implantation procedure).

2.2. Tumor models

All studies were approved by our institutional animal care and use committee and were performed in accordance with institutional guidelines. *Female athymic nude mice (BALB-c-nu/nu, 5–7 weeks old, 15–20 g, n = 15; Japan SLC, Inc., Hamamatsu, Japan) were introduced.* These mice were underwent the process of medical inspection and were given a resting period of one week after introducing. All mice were cared under facility-specific measure (SPF). PC-3 human prostate cancer cells were each visually injected at 1.0×10^6 cells/ml into both flakes (one for control, the other for IRE). These tumors were retained to be 10 mm in diameter to be suitable for IRE treatment procedures. Following growing of the tumor, these mice were randomly allotted as following time: 5, 12, 24, 72 h after IRE including the control, having 3 mice each time.

3. IRE procedures

3.1. IRE apparatus and dosing condition

An electropoator (Nano-porator; SolcoBiomedical Ltd., Co.) as an apparatus was used for IRE procedures with the following specifications: 1500 V output and 50 ampere at 100 μs pulse width maximum respectively, ranging from 100 μs to 100 ms for pulse duration, in accordance with the Korean Food and Drug Administration (KFDA) regulations. Two monopolar-electrodes were also used for all mice IRE procedures. Electrode array was constructed using two needles made of tungsten (each 50 mm in length with a diameter of 0.6 mm) whose surface was coated with pure-platinum through unbalanced magnetic field sputter of 10 μm in thickness without any toxicity. These electrodes were designed to be exposed only 4 mm in length and other parts were enveloped with a plastic blocker for insulation. They were inserted 4 mm into tumor tissues with 5 mm spacing between electrodes. Following previous studies [6],we chose 1.2 kVsquare wave pulses with 100 μs duration and 100 μs pulse interval to reduce thermal damage.

3.2. IRE procedure

Before IRE procedures, mice were anesthetized with Zoletil (Virbac, Carros, France) solution 10 mg/kg i.v. The two-parallel-electrode was put in one of the two tumors, being aligned along the axis of the largest tumor dimension on the site of mouse flake so that the electrodes can be positioned to thoroughly exert on the tumor. The electrodes were then wired to the electroporator and pulses were applied in pulse train mode. Following electrical application, the electrodes were pulled out and the tumor was inspected for bleeding, and care was taken if bleeding was present. Then the mice were moved in the SPF and bred until MRI.

3.3. MR images

Magnetic resonance imaging (MRI) was performed to evaluate the effects of IRE for some mice prior and at 12 and 72 h after the IRE procedures, using a 1.5-T clinical scanner (Magnetom Avanto; Siemens Medical Solutions, Erlangen, Germany). All MR images were taken without electrodes in the tumor tissues because the magnetic fields could be affected by the metallic electrodes. Thus, we did not identify localization of electrodes within tumor tissues for further imaging analysis. MRI scanning of the nude mice was performed in coronal plane. MR sequences included T1-weighted turbo spin-echo (TSE) images (repetition time [TR] ms/echo time [TE] ms, 300/8) and T2-weighted TSE images (TR/TE, 3500/60). The thickness was 2.0 mm, the space was 0.5 mm, the matrix was 256 × 256, and FOV was 150 mm. Contrast enhanced T1-weighted TSE images were also obtained after application of contrast agent via tail vein.

3.4. Histology

Following completion of MRI, the mice were anesthetized following the same protocol as above and the tumors were harvested from the mouse and stored in the solution of NBF (composed with formaldehyde, distilled water, NaH_2PO_4, and NaH_2PO_4). The mice were then finally euthanized. After fixing, the tumors were embedded in paraffin for histological examination. Tumor tissues were sliced in 4-μm-thick sections across the lesion including the control. These sections were stained with hematoxylin and eosin (H&E) staining and Terminal deoxynucleotidyl transferase dUTP nick end labeling (TUNEL), which is a method for detecting DNA fragmentation by labeling the terminal end of nucleic acids for apoptotic pathology. Histological slides were digitized with an image acquisition system (Olympus BX-51 with digital imaging system (Image-Pro plus 4.5)). Software (Matlab) for image analysis was employed to automatically qualify the region of interest containing areas of cellular necrosis on each image.

3.5. Simulation

For simulation of the ablation zone, we calculated the electric field by using a homemade C++ code. Following previous studies [7], we solved the equation $\nabla \cdot (\varepsilon \nabla \varphi) = \rho = 0$ using the relaxation method (Jackson, Classical Electrodynamics, 3rd ed.). The geometry of the problem was a 3 dimensional ellipsoid with two penetrating electrodes parallel to the z axis. The electric potential of the electrodes was ±600 V, and the potential of the surrounding environment was 0 V. The presented result (Fig. 1A) is the electric field over the cross section of the ellipsoid, cutting the ellipsoid into two equal parts in the x–y plane. We assumed the dielectric constant to be constant over the model organ. The dimension of the ellipsoid was 25 × 15 × 10 mm. We set a cubic lattice with a lattice constant of 0.2 mm. To present the result with higher accuracy, the cross section was interpolated using the gnuplot v. 4.4.

4. Results

All animals were alive during the experimental procedures, and showed no postoperative complications. The electrodes were inserted into the tumors along the long axis so that the applied electric fields could cover the entire tumors.

4.1. Apoptotic evaluation with post-IRE time

The IRE ablation area was in advance anticipated based on our electric field simulations for assessment of IRE ablation to cancerous tissues (Fig. 1A). Electric field is sharply localized between and beside electrodes. Based on such simulations, macroscopic evaluation of IRE-ablated lesions was performed using H&E staining and TUNEL assay at 5, 12, 24, and 72 h after IRE including the control. H&E staining and TUNEL assay showed clear aggressive progression post-IRE treatment (Fig. 1B) at all times. H&E images showed the irregular morphology of IRE treated tissues to the control. Necrosis can be distinguished between the electrode insertion sites. The TUNEL assay showed evidence of apoptosis by IRE, having brown color. Fig. 1C exhibits the result of apoptotic rate quantified the brown colored area by using Matlab. The peak apoptotic

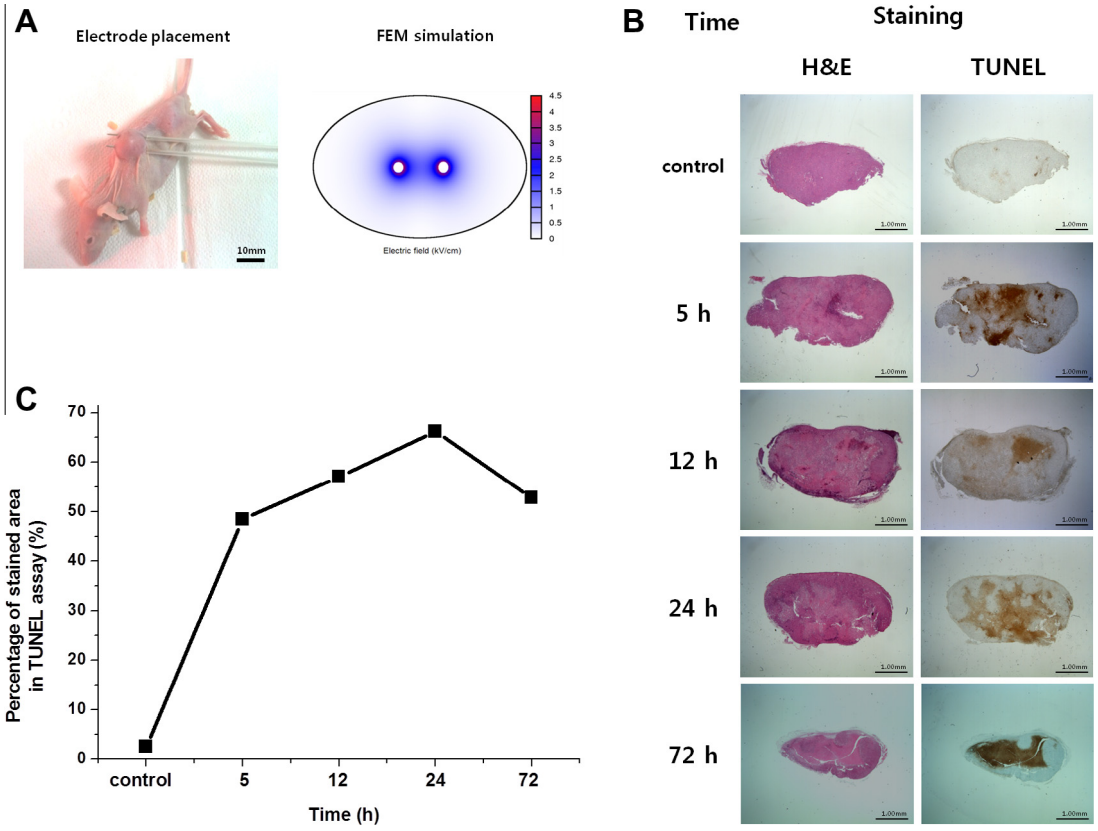

Fig. 1. The experimental setup and histological examination by IRE. (A) A photograph showing the electrode placement in tumor tissue with plastic tube protecting the mouse skin from electric shock and FEM simulation of applied IRE in condition of electric field 1.2 kV/cm, pulse duration 100 μs, pulse interval 100 μs, and applied pulse number 32. (B) Macroscopic images of sections of IRE-treated PC-3 tumor with H and E staining (left images) and TUNEL assay (right images). Images were taken after 5, 12, 24, and 72 h of IRE operation including the control. (C) A graph showing the ratio of the stained area in TUNEL assay. The apoptotic rate shows a peak at 24 h post-IRE.

rate was recorded at 24 h post-IRE and then decreased at 72 h post-IRE.

4.2. Microscopic evaluation of tumor microenvironment

Microscopic evaluation of the tumor microenvironment in the IRE-ablated area was first conducted in the center (between electrodes) and the border at all times. The left figures in Fig. 2A show extensive necrotizing tissues between the electrodes compared to the control, in which not many live cells seem to remain due to focusing of strong pulse electric fields. Grossly, a well-demarcate margin was visualized between treated and untreated tissues at the border of the tissues in the right figures. The untreated part of the demarcated margin with skin tissues was from where the pulse electric fields did not make a strong influence.

Fig. 2B reveals changes in the microenvironment of tumor tissues at the cellular level after IRE. The blood capillary (Fig. 2B (2)) was preserved after IRE compared to one of the controls (Fig. 2B (1)), whereas some hemorrhage caused by IRE can be seen (Fig. 2B (3)). Most cells that were in the tissues under IRE underwent pyknosis (Fig. 2B (2), arrowhead) and some of them *karyorhexis* (Fig. 2B (3), arrows), which is the irreversible process of chromatin condensation in the nucleus of cells undergoing apoptosis. Additionally, connective tissues (collagens) that were under IRE were mostly ruptured as shown in Fig. 2B [6], compared to the control (Fig. 2B (5)).

4.3. MR imaging evaluation

Representative MR images are shown in Fig. 3 with the corresponding HE staining images at 12 and 72 h post-IRE. Pre-IRE MR scanning in some mice showed homogeneous enhancement of tumor tissues without significant internal necrosis. MR scanning obtained after IRE procedures revealed that tumors affected by IRE demonstrated no enhancement after contrast administration intravenously. It indicates that most parts of the tumors are effectively devascularized, or, in other word, ablated. However, some cases showed prominent peripheral enhancement around the tumors. It could be reactive hyperemia, especially in immediate follow-up, or residual viable tumor tissues at the margin of the tumors, which can be confirmed by histological analysis. The IRE ablation zone was estimated by measuring the size of non-enhancing portion in the whole tumor.

5. Discussion

IRE is a novel method for ablation of living tissues due to its non-thermal effects during the process, which gives IRE another advantage of making a quick recovery [8]. This advantage of IRE is critical in which this method could be useful in treating almost all organs with tumor tissues. We applied the IRE to tumor tissues grown with prostate cancer cells. In our study, we successfully demonstrated changes with time within these tumor tissues that underwent IRE, and we confirmed apoptosis and/or necrosis as the results of IRE through histologic examination and contrast-enhanced T1-weighted images. Tissues under IRE ablation macroscopically showed clear aggressive changes at all times (5, 12, 24, and 72 h after IRE ablation) at histologic examination. We were thus able to observe delineating two separate zones; a central zone of IRE and a peripheral zone. Especially we could see changes in area post the IRE with time at TUNEL assay. These changes made it possible to quantify the areas with time. At 24 h after IRE

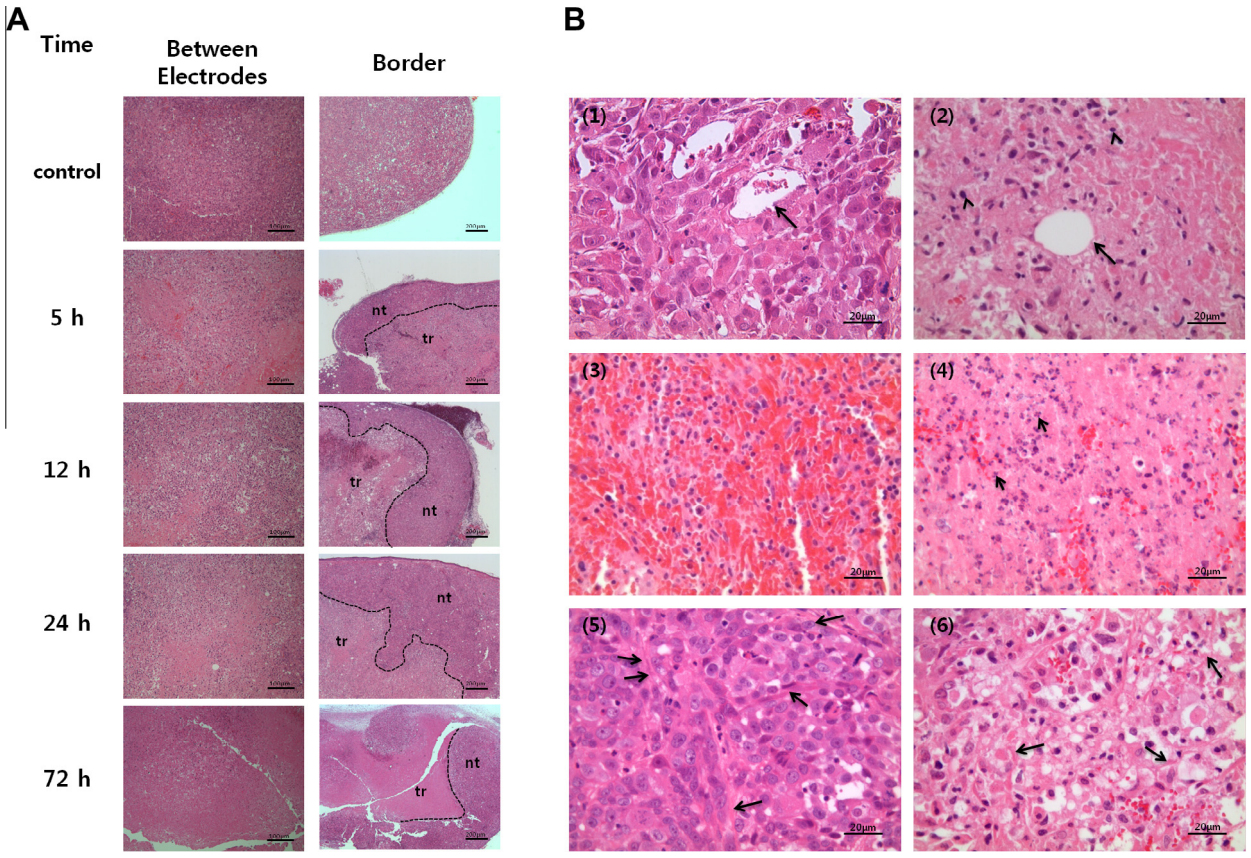

Fig. 2. Microscopic images of H and E staining. (A) The tissues between electrodes were not seen live. Marginal sections were at the border for all samples. Images were taken after 5, 12, 24, and 72 h of IRE operation including the control. (B) Typical images under apoptosis. The normal tissue shows the preserved capillaries (1), while the one destructed by IRE showed a chromatin condensations (arrow heads) but the preserved capillary (arrow) (2), other sites of the tissue are characterized as adventitial hemorrhage and pyknosis (3), and *karyorhexis* (4, arrows), which is the irreversible condensation of chromatin in the nucleus of cells undergoing apoptosis. The image (5) and (6) show extracellular matrix (arrow) of normal tissue of the control and destructed matrix (arrow) by IRE, respectively. All images were magnified to 40×.

treatment the analysis of TUNEL assay recorded a peak apoptotic rate. Since then the apoptotic rate decreased, which means natural degradation of apoptotic cells and phagocytosis by existing viable cells took place within the treated tissues.

Meanwhile, the peripheral rim of the treated tissues appeared viable. This viability might likely contribute to the falling of the apoptotic rate at 72 h after IRE ablation. This tendency may be consistent with the analysis, in which the border of the untreated area at 24 h post-IRE was greater than ones before 24 h. In spite of such a sure apoptotic peak at 24 h post-IRE in this study, according to a previous study on liver tissues [6], the rate was highest at 10 h after IRE and significantly decreased thereafter. This difference might be due to the disparity in vascular system and homeostatic system between tumor tissues and liver tissues [9]. Another reason might be speculated that irreversibly electroporated cells in tumor tissues were much greater than liver tissues because of a existing gradient of electric field potentials surrounding IRE treatment zones due to different electric impedance between them, while further studies are clearly necessary to elucidate the exact mechanisms for this difference [10].

Due to these different tissue properties, unlike liver tissues, we had difficulty in quantifying the apoptotic rate of tumor tissues with time in the TUNEL assay image. We anticipated that strongly pulsed electric fields would have influence on tumor tissues only between electrodes with the little peripheral rim of the electrode as expected in simulation (Fig. 1A). However IRE treatment induced apoptosis through entire tumor tissue unlike in a liver tissue [6]. Even we could not exactly find the location of the electrodes for the purpose of evaluating apoptosis between electrodes. In addition, natural apoptosis occurred more in control tumor tissues than liver tissue. These phenomena may be ascribed to the difference in the electric impedance of two tissues. Thus, we performed an evaluation involving the rate of the thoroughly apoptosis-measured area to the whole tissue region for convenience to disregard the different tissue size. It is yet unclear why there was no consistency in the effects between pathologic measurements and prediction by simulation.

Alterations in the tumor microenvironment as the results of apoptotic or necrotic changes with time by IRE ablation were microscopically evaluated. As with other results [11–13], there were extensive necrotizing, well-demarcated margin, preserved blood capillaries, hemorrhage, pyknosis, *karyorhexis*, and rupture of connective tissues. Here, blood capillary that was preserved might clearly remain basal lamina. This, afterward, may enable circulation of nutrients as a part of microcirculation so that tumor tissue may be alive. These microenvironmental changes served as great contrast features in contrast-enhanced MR images. We were consistently able to observe hypointense lesions in all IRE-treated tumors in all mice. These unenhanced zones were correlated with corresponding histologic images. On contrast-enhanced MR images, the tumor mass showed that the electric fields had thoroughly influenced the tissues than expected as mentioned above.

Our study had limitations. First, the analysis of apoptosis was depended only on a TUNEL assay method. Owing that the analysis

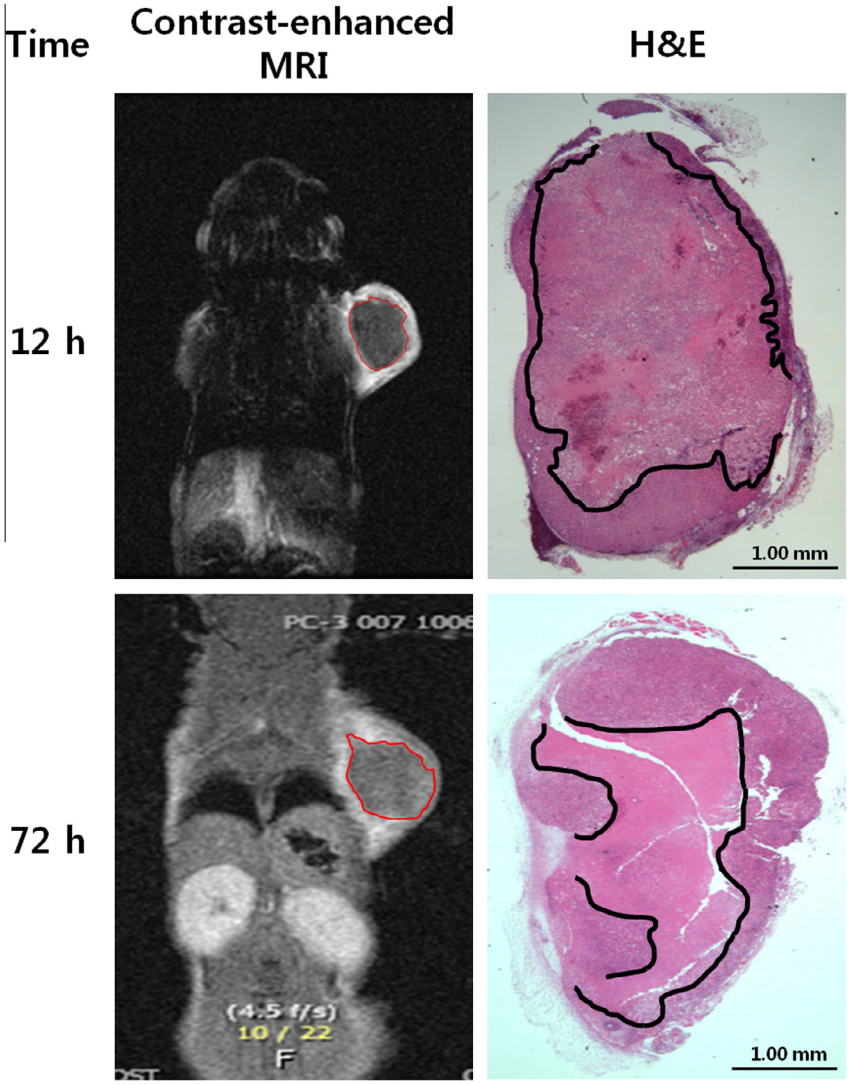

Fig. 3. Contrast-enhanced MR images and correspondingly H and E images, acquired at 12 and 72 h post-IRE. The MR images show uniformly hypointense lesions indicating that tissues were devascularized. Delineated lines in the images correspond to border between ablated and not-ablated areas.

is a method for detecting DNA fragmentation, apoptotic cells only by IRE could not be differentiated from natural apoptotic cells that was naturally being degraded. A second limitation of this study was that we did not take a long time (over a month) enough to observe a complete regression of tumor. *A third limitation lied in use of a nude mouse without an intact immune system in this study. As previous study* [1]*, we could not observe activations of the immune system by IRE and then get a potentially beneficial immune response into our results.*

Even though we had several limitations in our study, we investigated tissue changes with time by IRE ablation and the resulting apoptosis and/or necrosis was confirmed via MR-imaging. We showed that tumor tissues can be damaged more than normal liver tissues by IRE, blood capillaries were kept intact during IRE, and the apoptotic tumor cells began to be removed after 24 h. This result should support the validity of IRE as a cancer therapeutic tool.

Acknowledgments

This work was supported by Grant No. 03-2009-0210 from the SNUH research fund and Grant No. 03-2009-8 from the Boramae medical center research fund, and partially by No. 2010-0029418 from the Korean Government.

References

[1] B. Rubinsky, G. Onik, P. Mikus, Irreversible electroporation: a new ablation modality-clinical implications, Technol. Cancer Res. Treat. 6 (2007) 37–48.
[2] A. Golberq, M.L. Yarmush, Nonthermal irreversible electroporation: fundamentals, applications, and challenges, IEEE Trans. Biomed. Eng. 60 (2013) 707–714.
[3] Y. Zhang, Y. Guo, A.B. Ragin, R.J. Lewandowski, G.Y. Yang, G.M. Nijm, A.V. Sahakian, R.A. Omary, A.C. Larson, MR imaging to assess immediate response to irreversible electroporation for targeted ablation of liver tissues: preclinical feasibility studies in a rodent model, Radiology 256 (2010) 424–432.
[4] E.W. Lee, C. Chen, V.E. Prieto, S.M. Dry, C.T. Loh, S.T. Kee, Advanced hepatic ablation technique for creating complete cell death: irreversible electroporation, Radiology 255 (2010) 426–433.
[5] C.R. Schmidt, P. Shires, M. Mootoo, Real-time ultrasound imaging of irreversible electroporation in a porcine liver model adequately characterizes the zone of cellular necrosis, HPB (Oxford) 14 (2012) 98–102.
[6] Y.S. Choi, H.B. Kim, J. Chung, H.S. Kim, J.H. Yi, J.K. Park, Preclinical analysis of irreversible electroporation on rat liver tissues using a microfabricated electroporator, Tissue Eng. Part C Methods 16 (2010) 1245–1253.
[7] J.F. Edd, R.V. Davalos, Mathematical modeling of irreversible electroporation for treatment planning, Technol. Cancer Res. Treat. 6 (2007) 275–286.
[8] W. Zhou, Z. Xiong, Y. Liu, C. Yao, C. Li, Low voltage irreversible electroporation induced apoptosis in HeLa cells, J. Cancer Res. Ther. 8 (2012) 80–85.
[9] A.R. Pries, A.J. Cornelissen, A.A. Sloot, M. Hinkeldey, M.R. Dreher, M. Höpfner, M.W. Dewhirst, T.W. Secomb, Structural adaptation and heterogeneity of normal and tumor microvascular networks, PLoS Comput. Biol. 5 (2009) e1000394.

[10] Y. Guo, Y. Zhang, G.M. Nijm, A.V. Sahakian, G.Y. Yang, R.A. Omary, A.C. Larson, Irreversible electroporation in the liver: contrast-enhanced inversion-recovery MR imaging approaches to differentiate reversibly electroporated penumbra from irreversibly elecctroporated ablation zones, Radiology 258 (2011) 461–468.
[11] T.P. Kingham, A.M. Karkar, M.I. D'Angelica, P.J. Allen, R.P. Dematteo, G.I. Getrajdman, C.T. Sofocleous, S.B. Solomon, W.R. Jarnagin, Y. Fong, Ablation of perivascular hepatic malignant tumors with irreversible electroporation, J. Am. Coll. Surg. 215 (2012) 379–387.
[12] E. Ben-David, L. Appelbaum, J. Sosna, I. Nissenbaum, S.N. Goldberg, Characterization of irreversible electroporation ablation in *in vivo* porcine liver, Am. J. Roentgenol. 198 (2012) 62–68.
[13] G. Narayanan, Irreversible electroporation for treatment of liver cancer, Gastroenterol. Hepatol. (NY) 7 (2011) 313–316.